Spectrum of the Nuclear Environment for GaAs Spin Qubits

Filip K. Malinowski,[1] Frederico Martins,[1] Łukasz Cywiński,[2] Mark S. Rudner,[1,3] Peter D. Nissen,[1] Saeed Fallahi,[4] Geoffrey C. Gardner,[4,5] Michael J. Manfra,[6,7] Charles M. Marcus,[8] and Ferdinand Kuemmeth[1]

[1]*Center for Quantum Devices, Niels Bohr Institute, University of Copenhagen, 2100 Copenhagen, Denmark*
[2]*Institute of Physics, Polish Academy of Sciences, Aleja Lotnikow 32/46, PL-02668 Warsaw, Poland*
[3]*Niels Bohr International Academy, Niels Bohr Institute, 2100 Copenhagen, Denmark*
[4]*Department of Physics and Astronomy, Birck Nanotechnology Center, Purdue University, West Lafayette, Indiana 47907, USA*
[5]*School of Materials Engineering and School of Electrical and Computer Engineering, Purdue University, West Lafayette, Indiana 47907, USA*
[6]*Department of Physics and Astronomy, Birck Nanotechnology Center, and Station Q Purdue, Purdue University, West Lafayette, Indiana 47907, USA*
[7]*School of Materials Engineering, Purdue University, West Lafayette, Indiana 47907, USA*
[8]*Center for Quantum Devices and Station Q Copenhagen, Niels Bohr Institute, University of Copenhagen, 2100 Copenhagen, Denmark*

(Received 6 January 2017; published 28 April 2017)

Using a singlet-triplet spin qubit as a sensitive spectrometer of the GaAs nuclear spin bath, we demonstrate that the spectrum of Overhauser noise agrees with a classical spin diffusion model over 6 orders of magnitude in frequency, from 1 mHz to 1 kHz, is flat below 10 mHz, and falls as $1/f^2$ for frequency $f \gtrsim 1$ Hz. Increasing the applied magnetic field from 0.1 to 0.75 T suppresses electron-mediated spin diffusion, which decreases the spectral content in the $1/f^2$ region and lowers the saturation frequency, each by an order of magnitude, consistent with a numerical model. Spectral content at megahertz frequencies is accessed using dynamical decoupling, which shows a crossover from the few-pulse regime ($\lesssim 16\pi$ pulses), where transverse Overhauser fluctuations dominate dephasing, to the many-pulse regime ($\gtrsim 32\,\pi$ pulses), where longitudinal Overhauser fluctuations with a $1/f$ spectrum dominate.

DOI: 10.1103/PhysRevLett.118.177702

Precise control of single electron spins in gate-defined quantum dots makes them a promising platform for quantum computation [1–5]. In particular, GaAs spin qubits benefit from unmatched reliability in fabrication and tuning. However, being a III–V semiconductor, the GaAs lattice hosts spinful nuclei that couple to electron spins via the hyperfine interaction [3,5–8]. Nuclear dynamics lead to fluctuations of the Overhauser field, which affect the coherent evolution of spin qubits. In turn, advances in qubit operation, including single-shot readout [9] and long dynamical decoupling sequences [6], allow spin qubits to serve as sensitive probes of the electron-plus-nuclear-environment system, an interesting coupled nonlinear many-body system.

In this Letter, we use a singlet-triplet ($S - T_0$) qubit as a probe to reveal the dynamics and magnetic field dependence of the GaAs nuclear spin bath over a wide range of frequencies, without the use of nuclear pumping [10–12] or postselection [13] techniques. The qubit is defined in a two-electron double quantum dot [Fig. 1(a)]. The external magnetic field B_{ext} separates the qubit states singlet, $|S\rangle = (1/\sqrt{2})(+|\uparrow\downarrow\rangle - |\downarrow\uparrow\rangle)$, and the unpolarized triplet, $|T_0\rangle = (1/\sqrt{2})(|\uparrow\downarrow\rangle + |\downarrow\uparrow\rangle)$, from the fully polarized triplet states, $|T_+\rangle = |\uparrow\uparrow\rangle$ and $|T_-\rangle = |\downarrow\downarrow\rangle$. In this notation, the first (second) arrow indicates the spin in the left (right) dot. The resulting energy diagram of the spin states at the transition between (1,1) and (2,0) charge states is presented in Fig. 1(b). Here (N, M) indicates the number of electrons in the left (N) and the right (M) dot. The Bloch sphere representation of the qubit is shown in Fig. 1(c).

Dynamics of the $S - T_0$ qubit in the well-separated (1,1) charge state, i.e., for vanishing exchange J between the two electrons, is governed by the static external magnetic field B_{ext} and dynamic Overhauser fields. For large B_{ext}, we can model the qubit evolution using the Hamiltonian [6,7,14]

$$\hat{H}(t) = g\mu_B \sum_{i=L,R} \left(B^i_{\parallel}(t) + \frac{|\mathbf{B}^i_{\perp}(t)|^2}{2|B_{\mathrm{ext}}|} \right) \hat{S}^i_z, \qquad (1)$$

where $g \sim -0.4$ is the electronic g factor, μ_B is a Bohr magneton, $\hat{S}^i_z$ is the spin operator of the electron in left or right dot $i = L$, R, and $B^i_{\parallel}$ is the Overhauser field component parallel to B_{ext}. The influence of the transverse Overhauser field component $\mathbf{B}^i_{\perp}$ on the qubit is strongly suppressed when B_{ext} is much larger than the typical Overhauser field. Hence, the transverse Overhauser field fluctuations play a significant role in the qubit evolution only when the influence of the fluctuating longitudinal Overhauser field $B^i_{\parallel}$ is eliminated by dynamical decoupling [6,7]. The splitting between qubit states $|\downarrow\uparrow\rangle$ and $|\uparrow\downarrow\rangle$ for $J = 0$ is thus proportional to the longitudinal component of the Overhauser field gradient, $\Delta B_{\parallel} = B^L_{\parallel} - B^R_{\parallel}$, and can be measured by monitoring the qubit precession between $|S\rangle$ and $|T_0\rangle$ [8,9,15].

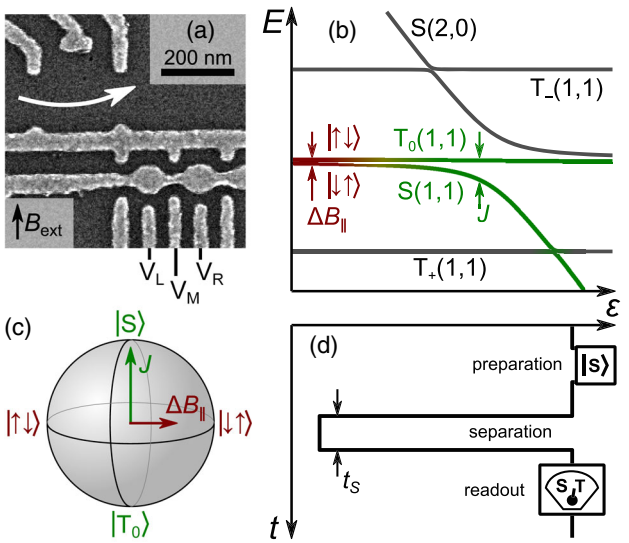

FIG. 1. (a) Electron micrograph of the device. Gate voltages V_i control the double dot state on ns time scales. Reflectance from the rf resonant circuit incorporating a sensor dot (white arrow) measures the charge state of the double dot located below the round accumulation gates. (b) Energy levels of the two-electron double dot as a function of detuning $\varepsilon = V_L - V_R$ at the (1,1)–(2,0) charge transition. Red-green lines indicate the qubit states. (c) Bloch sphere representation of the qubit. Rotation axes correspond to exchange interaction J (green) and gradient of the Overhauser field $\Delta B_\parallel$ (red). (d) Pulse cycle used to probe the qubit precession in the gradient of the Overhauser field. The qubit is initialized in the $S(2,0)$ state by exchanging electrons with the lead. Next, one electron is moved to the right dot, and the qubit evolves for the time t_S in the gradient of the Overhauser field. Finally, ε is pulsed back to the readout point, projecting $|S\rangle$ into a (2,0) charge state, whereas $|T_0\rangle$ remains in (1,1).

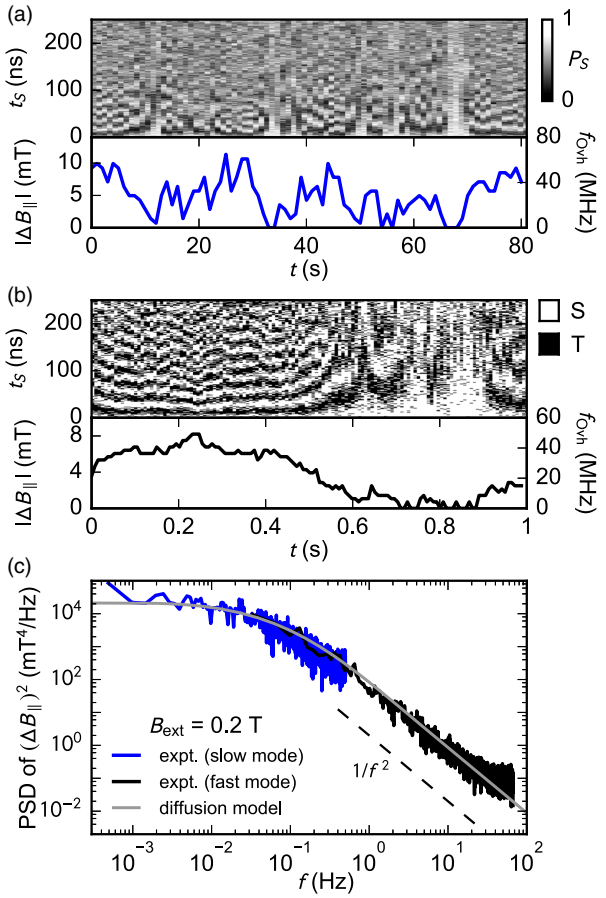

FIG. 2. (a),(b) Top panels present $S - T_0$ oscillations resulting from the relative precession of the two electron spins in the Overhauser field gradient, as a function of laboratory time at $B_{ext} = 0.2$ T (see main text). In the bottom panels we show the extracted frequency of oscillations, f_{Ovh}, converted to $|\Delta B_\parallel|$. (c) Power spectral density of $(\Delta B_\parallel)^2$ at $B_{ext} = 0.2$ T obtained from traces such as in (a) (blue) and (b) (black). Transition from white spectrum at low frequencies to $1/f^2$ at high frequencies is reproduced by the nuclear spin diffusion model (gray). A deviation from this dependence at the highest frequencies is a numerical artifact caused by the discreteness of $|\Delta B_\parallel|$ values obtained from the Fourier analysis.

To measure this precession, we apply a cyclic pulse sequence that first prepares the singlet, then separates the two electrons to allow free precession in the Overhauser field for time t_S, and, finally, performs a projective readout of the qubit in the $S - T_0$ basis [Fig. 1(d)]. The total length of the pulse sequence is approximately 30 μs, including 10 μs of readout time. For each t_S we use 16 single-shot readouts of this sequence to estimate the singlet return probability, P_S. Repeatedly sweeping t_S from 0 to 250 ns in 300 steps allows the precession of the qubit in the evolving Overhauser field to be measured with roughly 1 s temporal resolution (slow mode). A time trace showing 80 s of slow-mode probability data is shown in Fig. 2(a). To increase the temporal resolution from 1 s to 12 ms we omit the probability estimation and record one single-shot outcome for each t_S (fast mode). A time trace showing 1 s of fast-mode single-shot data is shown in Fig. 2(b). The time evolution of the qubit precession frequency, $f_{Ovh}(t)$, is then extracted from these data as described in the Supplemental Material [16], Sec. I. The frequency corresponds to the absolute value of the Overhauser field gradient $|\Delta B_\parallel(t)| = hf_{Ovh}(t)/|g|\mu_B$. Examples of $|\Delta B_\parallel(t)|$ for $B_{ext} = 0.2$ T are shown in Figs. 2(a), 2(b). In contrast to experiments performing dynamic nuclear polarization [17–19] the observed distributions of $\Delta B_\parallel$ reveal no sign of multistable behavior (see Supplemental Material [16], Sec. II).

Next, we focus on the power spectral density (PSD) of $\Delta B_\parallel$ for $B_{ext} = 0.2$ T. Since taking the absolute value of $\Delta B_\parallel$ introduces kinks in $|\Delta B_\parallel|$ traces, adding spurious high-frequency content, we instead extract the PSD of $(\Delta B_\parallel)^2$ [Fig. 2(c)]. The resulting spectrum is flat below 10^{-2} Hz and falls off as $1/f^2$ above 1 Hz, indicating a correlation time of $\Delta B_\parallel$ of a few seconds.

A classical model of Overhauser field fluctuations due to nuclear spin diffusion is used to fit the experimental data in Fig. 2(c) [20] (Supplemental Material [16], Sec. V). In the model we use the double dot geometry estimated from the lithographic dimensions of the device and the

heterostructure growth parameters (distance between the dots $d = 150$ nm, dot diameter $\sigma_\perp = 40$ nm and width of the electron wave function in the crystal growth direction $\sigma_z = 7.5$ nm). We fit the effective diffusion constant $D = 33$ nm^2/s and the equilibrium width of the $\Delta B_\parallel$ distribution $\sigma_{\Delta B} = 6.0$ mT. This model yields the power spectrum of $\Delta B_\parallel$, which has the same qualitative behavior as the spectrum of $(\Delta B_\parallel)^2$—it is flat at low frequencies ($< 10^{-2}$ Hz) and falls off as $1/f^2$ at high frequencies (> 1 Hz). Such a relation between the PSD of a Gaussian distributed variable and that of its square is expected whenever the PSD has a $1/f^\beta$ dependence over a wide frequency range [21].

In order to extend the spectral range to higher frequencies we apply the pulse cycle with a fixed separation time $t_S = 100$ ns, acquiring a single-shot measurement every 30 μs. This can be visualized as a horizontal cut through the data in Fig. 2(b) (top) at 100 ns, though, of course, now without taking the rest of the data at other values of t_S. Although the series of single-shot outcomes at fixed t_S does not allow a direct measure of $\Delta B_\parallel$ from temporal oscillations, it does give statistical spectral information [20]. In particular, the Fourier transform of the windowed autocorrelation of single-shot outcomes (Supplemental Material [16], Sec. III) yields a PSD of the singlet return probability P_S, now extended to 4 kHz.

Power spectra of P_S for the lowest and highest applied fields studied, $B_{\text{ext}} = 0.1$ and 0.75 T are shown in Fig. 3. We observe that the spectrum for $B_{\text{ext}} = 0.75$ T is reduced by an order of magnitude in the $1/f^2$ regime, compared to the spectrum at $B_{\text{ext}} = 0.1$ T. To quantify the observed magnetic field dependence of the PSD of P_S we fit the nuclear spin diffusion constant D of the classical diffusion model (Supplemental Material [16], Sec. V) to data, using fixed $\sigma_{\Delta B} = 6.0$ mT (obtained from the fit in Fig. 2) and the same geometrical parameters as above. The observed

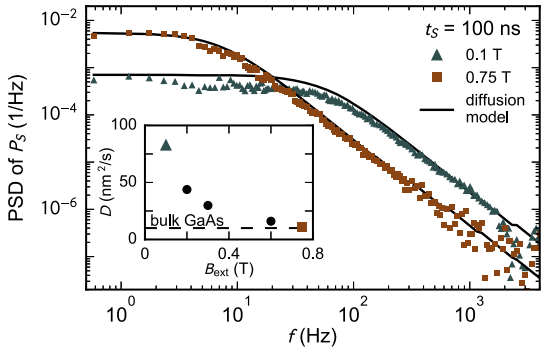

FIG. 3. Magnetic field dependence of the power spectral density of P_S, keeping $t_S = 100$ ns fixed. Increasing B_{ext} from 0.1 to 0.75 T suppresses the $1/f^2$ noise by an order of magnitude. Solid lines are fits of the diffusion model with the effective diffusion constant D being the only free parameter. Inset: D as a function of magnetic field B_{ext}. Dashed line indicates the spin diffusion constant for bulk GaAs, $D = 10$ nm^2/s [22].

agreement with experimental data suggests that the effects of the nuclear spin bath are well described by classical evolution up to at least 1 kHz.

At low B_{ext} we observe a strong enhancement of the effective spin diffusion constant compared to the literature value for bulk GaAs in the absence of free electrons, $D \sim 10$ nm^2/s [22] (Fig. 3, inset). Qualitatively, this increase may be attributed to electron-mediated nuclear flip-flop processes [20,23–26], which dominate over nuclear dipole-dipole mediated diffusion. At 0.75 T the effective diffusion constant drops down to the value for bulk GaAs. Despite this agreement, we note that our values for D are not corrected for possible changes of electronic wave functions with increasing magnetic field. A quantitative statement about the underlying bare diffusion constant is difficult, as the fitting results for D are sensitive to assumptions about the spatial extent of the quantum dots (in particular $\sigma_\perp$) and the fraction of time spent in (1,1) and (2,0). Since spin diffusion due to nuclear dipole-dipole interaction is strongly suppressed by the Knight field gradient [27] and quadrupolar splittings, we expect further suppression of D at higher magnetic fields [25], and saturation below the bulk GaAs value. Indeed, this is observed in self-assembled quantum dots, where quadrupolar splittings are significantly stronger due to strain [24,28,29].

Overhauser field fluctuations above 100 kHz are too fast to be observed as oscillation between $|S\rangle$ and $|T_0\rangle$ with the present setup. However, we can infer spectral features from the decoherence of $|\uparrow\downarrow\rangle$ and $|\downarrow\uparrow\rangle$ states using Hahn echo and Carr-Purcell-Meiboom-Gill (CPMG) dynamical decoupling sequences [6,30]. Since these decoupling sequences act as filters in the frequency domain, we can relate the Overhauser spectrum to the decay of qubit coherence [6,31–33]. In particular, Hahn echo and CPMG sequences suppress the low frequency fluctuations, making the coherence decay a sensitive probe of high-frequency Overhauser fields.

The decoupling sequence in Fig. 4(a) uses symmetric exchange pulses [34], but is otherwise standard [30]: initialize in $S(2,0)$, evolve for time $\tau/2$ in (1,1), apply symmetric exchange π pulse, evolve for another $\tau/2$, repeat the $\tau/2 - \pi - \tau/2$ segment a total of n times. After the total evolution time $T = n\tau$, project onto $S - T_0$ by pulsing to (2,0) and perform single-shot readout. Averaging $\sim$1000 such single-shot readouts then yields the singlet return probability. For such a sequence the resulting singlet return probability is related to the qubit coherence by $P_S = \frac{1}{2} + \frac{1}{2}\text{Re}[W_L(n\tau)W_R^*(n\tau)]$, where $W_i(t)$ is the normalized coherence of the spin in dot i at time t.

Figure 4(b) shows the singlet return probability for Hahn echo and CPMG sequences with various numbers of π pulses n as a function of the interpulse time $\tau = T/n$. For sequences with small n, coherence decreases smoothly with τ, while for sequences with large n the decay is strongly modulated. It was previously shown [6,7] that the coherence modulations are due to narrow-band spectral content

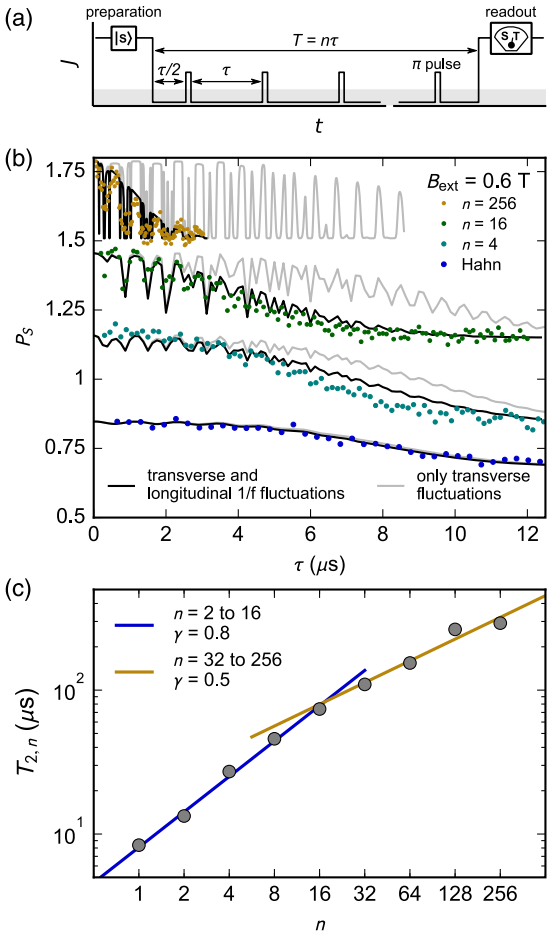

FIG. 4. (a) Schematic of a CPMG dynamical decoupling sequence applied to a $S-T_0$ qubit, presented as a time dependent exchange energy J (see text). (b) Coherence of the $S-T_0$ qubit after Hahn echo and CPMG sequences with number of π pulses n. $\tau = T/n$ is the repetition period between pulses. Black curves present simulations including longitudinal $1/f$ noise and transverse fluctuations due to Larmor precession of the nuclei. Gray curves assume transverse Overhauser field fluctuations only. Data and curves are offset for clarity. (c) Scaling of the extracted coherence decay envelope $T_{2,n}$ with n. Solid blue and yellow lines indicate fits of the power law $\propto n^{\gamma}$ to data in the indicated range. A large value of $\gamma = 0.8$ for small number of π pulses indicates that decay is dominated by the transverse noise. $\gamma = 0.5$ for large n is consistent with decay due to longitudinal $1/f$ noise.

at megahertz frequencies in the transverse Overhauser field $\mathbf{B}^i_\perp$, arising from the relative Larmor precession of the three nuclear species.

The influence of transverse Overhauser fluctuations $\mathbf{B}^i_\perp$ on the CPMG signal decay was simulated using a semiclassical theory [14,35,36] that previously gave good agreement with echo [18,37] and CPMG [6] experiments (see Supplemental Material [16], Sec. VI for details). Comparisons of experimental data with numerical simulations are shown in Fig. 4(b). First, we include only narrow-band transverse fields (gray curves), assuming two identical dots each containing $N = 9 \times 10^5$ nuclei and a spread of effective fields experienced by the nuclei of $\delta B = 1$ mT, arising, for example, from quadrupolar splittings [7,37,38]. This simulation reproduces the coherence decay for Hahn echo and the coherence modulations. The decay envelopes for the simulated CPMG, however, do not agree well with experiment, especially for large n. In order to gain additional insight into the source of decoherence we extract the envelope decay time $T_{2,n}$ from the experimental data and plot it as a function of n [Fig. 4(c) and Supplemental Material [16], Fig. S4] [30]. We observe an initial scaling of $T_2^{\mathrm{CPMG}} \propto n^{\gamma}$ with $\gamma \sim 0.8$, and a crossover to $\gamma \sim 0.5$ for large n.

We ascribe the change in the observed T_2^{CPMG} scaling to a crossover between decoherence limited by transverse to longitudinal Overhauser field dynamics. For small n the fluctuations of $\mathbf{B}^i_\perp$ dominate the decoherence, leading to scaling with large γ; purely transverse low-frequency fluctuations are expected to yield $T_2^{\mathrm{CPMG}} \propto n^{\gamma}$ with $\gamma = 1$ (see Supplemental Material [16], Sec. VI). With increasing n other decoherence sources start playing a dominant role. The intermediate-frequency fluctuations of $\Delta B_\parallel$ cause additional superexponential decay, which for large n is given by $\exp[-4TS_\parallel(1/2\tau)/\pi^2]$, where $S_\parallel(f)$ is the PSD of $\Delta B_\parallel$ [39–41]. Assuming that this PSD has a $1/f^{\beta}$ power-law behavior in the relevant frequency range, the CPMG decay for fixed n and varying τ is then $\exp[-(T/T_{2,n})^{\beta+1}]$, with $T_{2,n} \propto n^{\gamma}$ and $\gamma = \beta/(\beta+1)$ [30]. The observed scaling with $\gamma \sim 0.5$ is, therefore, consistent with $1/f$ noise and a Gaussian decay.

As shown in Fig. 4(b) (black lines), adding the $\beta = 1$ envelope function, $\exp[-(T/T_{2,n})^2]$ and $T_{2,n} = n^{1/2} \times 25\,\mu$s, appropriate for $\beta = 1$, gives good agreement with experimental results. From the agreement between the simulations and the measurements we estimate that for $f > 100$ kHz the PSD $S_\parallel(f) \sim A^2/(2\pi f)$ with $A^{-1} \sim 9\ \mu$s. For comparison with results presented in Ref. [6] we extrapolate this frequency dependence to 667 kHz. Using the extrapolated value we estimate the CPMG decay time in an experiment in which τ is fixed but n is varied, $T_2^{\mathrm{CPMG}} = \pi^2/4S_\parallel(1/2\tau)$. Such estimate yields $\approx$0.83 ms for $\tau = 750$ ns, which is close to $T_2^{\mathrm{CPMG}} = 0.87 \pm 0.13$ ms measured in Ref. [6].

The $1/f$ power law found for $f > 100$ kHz differs from the $1/f^2$ spectrum observed below 1 kHz. This is not surprising, since for frequencies higher than the strength of intranuclear interactions ($\sim$1 kHz) the diffusion model is no longer applicable. Whether the high-frequency $\Delta B_\parallel$ fluctuations have the same physical origin (i.e., flip flops of nuclei due to dipolar and hyperfine-mediated interactions) as the low-frequency ones is an open question.

Theory for CPMG decay caused by spectral diffusion due to dipolar interactions predicts a coherence decay of the form $\exp[-(T/T_{2,n})^6]$, with $T_{2,n} \propto n^{2/3}$ for small and even n [42]. This decay form (and scaling) is in disagreement with our observations. In particular. for large n, existing spectral diffusion theories based on cluster expansion [43–45] may need to be refined, for example, taking into

account realistic shapes of the electronic wave functions. Based on our findings, such theories can be tested experimentally at $B_{\mathrm{ext}} > 1$ T, where bare dipole-dipole coupling is the dominant internuclear interaction.

Finally, it is possible that the $\Delta B_{\parallel}$ fluctuations are not of intrinsic origin (nuclear dynamics), but of extrinsic origin. For example, charge noise, which generically has a $1/f^{\beta}$ spectrum with $\beta \sim 1$ [46], can shift the electron wave function and effectively result in Overhauser field fluctuations [14].

In conclusion, we have experimentally investigated the spectrum of the GaAs nuclear environment for spin qubits and find it consistent with classical diffusion over 6 orders of magnitude in frequency, from millihertz to kilohertz. For applied fields below ~0.75 T, nuclear diffusion is dominated by the electron-mediated flip flop, enhancing diffusion by a factor of 8. Decoherence of the $S - T_0$ qubit is dominated by fluctuations of the transverse Overhauser field for short CPMG sequences, and by longitudinal Overhauser field for CPMG sequences with more than 32π pulses.

This work was supported by the Army Research Office, the Polish National Science Centre (NCN) under Grants No. DEC-2012/07/B/ST3/03616 and No. DEC-2015/19/B/ST3/03152, the Innovation Fund Denmark, the Villum Foundation, and the Danish National Research Foundation.

[1] D. Loss and D. P. DiVincenzo, Phys. Rev. A **57**, 120 (1998).
[2] M. Veldhorst *et al.*, Nature (London) **526**, 410 (2015).
[3] J. R. Petta, A. C. Johnson, J. M. Taylor, E. A. Laird, A. Yacoby, M. D. Lukin, C. M. Marcus, M. P. Hanson, and A. C. Gossard, Science **309**, 2180 (2005).
[4] K. C. Nowack, M. Shafiei, M. Laforest, G. E. D. K. Prawiroatmodjo, L. R. Schreiber, C. Reichl, W. Wegscheider, and L. M. K. Vandersypen, Science **333**, 1269 (2011).
[5] M. D. Shulman, O. E. Dial, S. P. Harvey, H. Bluhm, V. Umansky, and A. Yacoby, Science **336**, 202 (2012).
[6] F. K. Malinowski *et al.*, Nat. Nanotechnol. **12**, 16 (2017).
[7] H. Bluhm, S. Foletti, I. Neder, M. S. Rudner, D. Mahalu, V. Umansky, and A. Yacoby, Nat. Phys. **7**, 109 (2011).
[8] S. Foletti, H. Bluhm, D. Mahalu, V. Umansky, and A. Yacoby, Nat. Phys. **5**, 903 (2009).
[9] C. Barthel, D. J. Reilly, C. M. Marcus, M. P. Hanson, and A. C. Gossard, Phys. Rev. Lett. **103**, 160503 (2009).
[10] M. D. Shulman, S. P. Harvey, J. M. Nichol, S. D. Bartlett, A. C. Doherty, V. Umansky, and A. Yacoby, Nat. Commun. **5**, 5156 (2014).
[11] A. Bechtold, D. Rauch, F. Li, T. Simmet, P.-L. Ardelt, A. Regler, K. Müller, N. A. Sinitsyn, and J. J. Finley, Nat. Phys. **11**, 1005 (2015).
[12] J. M. Nichol, S. P. Harvey, M. D. Shulman, A. Pal, V. Umansky, E. I. Rashba, B. I. Halperin, and A. Yacoby, Nat. Commun. **6**, 7682 (2015).
[13] M. R. Delbecq *et al.* Phys. Rev. Lett. **116**, 046802 (2016).
[14] I. Neder, M. S. Rudner, H. Bluhm, S. Foletti, B. I. Halperin, and A. Yacoby, Phys. Rev. B **84**, 035441 (2011).
[15] C. Barthel, J. Medford, H. Bluhm, A. Yacoby, C. M. Marcus, M. P. Hanson, and A. C. Gossard, Phys. Rev. B **85**, 035306 (2012).
[16] See Supplemental Material at http://link.aps.org/supplemental/10.1103/PhysRevLett.118.177702 for details about data analysis, nuclear spin diffusion model, and effects of transverse Overhauser noise.
[17] J. Danon, I. T. Vink, F. H. L. Koppens, K. C. Nowack, L. M. K. Vandersypen, and Y. V. Nazarov, Phys. Rev. Lett. **103**, 046601 (2009).
[18] H. Bluhm, S. Foletti, D. Mahalu, V. Umansky, and A. Yacoby, Phys. Rev. Lett. **105**, 216803 (2010).
[19] F. Forster, M. Mühlbacher, D. Schuh, W. Wegscheider, G. Giedke, and S. Ludwig, Phys. Rev. B **92**, 245303 (2015).
[20] D. J. Reilly, J. Taylor, E. A. Laird, J. Petta, C. M. Marcus, M. P. Hanson, and A. C. Gossard, Phys. Rev. Lett. **101**, 236803 (2008).
[21] L. Cywinski, Phys. Rev. A **90**, 042307 (2014).
[22] D. Paget, Phys. Rev. B **25**, 4444 (1982).
[23] D. Klauser, W. A. Coish, and D. Loss, Phys. Rev. B **78**, 205301 (2008).
[24] C. Latta, A. Srivastava, and A. Imamoglu, Phys. Rev. Lett. **107**, 167401 (2011).
[25] Z. X. Gong, Z. Q. Yin, and L. M. Duan, New J. Phys. **13**, 033036 (2011).
[26] D. J. Reilly, J. Taylor, J. Petta, C. M. Marcus, M. P. Hanson, and A. C. Gossard, Phys. Rev. Lett. **104**, 236802 (2010).
[27] C. Deng and X. Hu, Phys. Rev. B **72**, 165333 (2005).
[28] A. E. Nikolaenko *et al.*, Phys. Rev. B **79**, 081303(R) (2009).
[29] E. A. Chekhovich, M. Hopkinson, M. S. Skolnick, and A. I. Tartakovskii, Nat. Commun. **6**, 6348 (2015).
[30] J. Medford, L. Cywinski, C. Barthel, C. M. Marcus, M. P. Hanson, and A. C. Gossard, Phys. Rev. Lett. **108**, 086802 (2012).
[31] J. M. Martinis, S. Nam, J. Aumentado, K. Lang, and C. Urbina, Phys. Rev. B **67**, 094510 (2003).
[32] L. Cywinski, R. M. Lutchyn, C. P. Nave, and S. Das Sarma, Phys. Rev. B **77**, 174509 (2008).
[33] M. J. Biercuk, A. C. Doherty, and H. Uys, J. Phys. B **44**, 154002 (2011).
[34] F. Martins, F. K. Malinowski, P. D. Nissen, E. Barnes, S. Fallahi, G. C. Gardner, M. J. Manfra, C. M. Marcus, and F. Kuemmeth, Phys. Rev. Lett. **116**, 116801 (2016).
[35] L. Cywinski, W. M. Witzel, and S. Das Sarma, Phys. Rev. Lett. **102**, 057601 (2009).
[36] L. Cywinski, W. M. Witzel, and S. Das Sarma, Phys. Rev. B **79**, 245314 (2009).
[37] T. Botzem, R. P. G. McNeil, D. Schuh, D. Bougeard, and H. Bluhm, Nat. Commun. **7**, 11170 (2016).
[38] R. Stockill, C. Le Gall, C. Matthiesen, L. Huthmacher, E. Clarke, M. Hugues, and M. Atatüre, Nat. Commun. **7**, 12745 (2016).
[39] G. A. Álvarez and D. Suter, Phys. Rev. Lett. **107**, 230501 (2011).
[40] T. Yuge, S. Sasaki, and Y. Hirayama, Phys. Rev. Lett. **107**, 170504 (2011).

[41] J. Bylander, S. Gustavsson, F. Yan, F. Yoshihara, K. Harrabi, G. Fitch, D. G. Cory, Y. Nakamura, J.-S. Tsai, and W. D. Oliver, Nat. Phys. **7**, 565 (2011).
[42] W. M. Witzel and S. Das Sarma, Phys. Rev. Lett. **98**, 077601 (2007).
[43] W. M. Witzel and S. Das Sarma, Phys. Rev. B **74**, 035322 (2006).
[44] W. Yao, R. B. Liu, and L. J. Sham, Phys. Rev. B **74**, 195301 (2006).
[45] W. Yang and R. B. Liu, Phys. Rev. B **79**, 115320 (2009).
[46] O. E. Dial, M. D. Shulman, S. P. Harvey, H. Bluhm, V. Umansky, and A. Yacoby, Phys. Rev. Lett. **110**, 146804 (2013).